Stability and loss in an ion-trap resonator

H. B. Pedersen, D. Strasser, O. Heber, M. L. Rappaport, and D. Zajfman*
Department of Particle Physics, Weizmann Institute of Science, Rehovot 76100, Israel
(Received 10 July 2001; revised manuscript received 25 September 2001; published 18 March 2002)

The stability and ion loss in a linear electrostatic ion trap are investigated experimentally and by numerical simulations. The decay of a stored 4.2-keV Ar^+ beam was monitored for various potential configurations of the trap. Both classical trajectory calculations and optical models were used to numerically study the stability and dynamics of the trapped ions. Two different modes of trapping were identified with very different dynamical properties. It is found that the ion-loss processes are controlled by collisions both with residual gas species and among the stored ions.

DOI: 10.1103/PhysRevA.65.042703 PACS number(s): 34.80.Gs

I. INTRODUCTION

The application of ion traps and heavy-ion storage rings has had a significant impact on many branches of physics [1]. In these devices, ions are stored for a relatively long time, either as a cloud (with meV to eV kinetic energies, in ion traps) or as a high-kinetic-energy beam (with MeV kinetic energies, in heavy-ion storage rings). For ion-trap devices, such as the Paul trap (quadrupole trap) [2,3], the Penning trap [4,5], the Paul-Straubel trap [6,7], the static [8,9] and dynamic Kingdon trap [10,11], ions are confined using static or time-dependent electromagnetic fields. On the other hand, in heavy-ion storage rings, the energetic ions are confined using large-scale static magnetic structures.

Recently, electrostatic ion traps for storage of fast ions with keV energies have been developed. The first of these devices [12,13] was designed as a resonator in which ions oscillated between a pair of electrostatic mirrors. Similar designs based on the same principle, but using slightly different types of reflecting electrodes, have been built [14–17]. An electrostatic storage ring has also been set up [18], which allows for the storage of keV ion beams. Among the advantages of these devices are that they are relatively small and that, since the confinement of ions is achieved using only electrostatic fields, there are no limits for the masses of the ions that can be stored. Several experiments have already been performed with these devices, such as metastable-state lifetime measurements [19,20], lifetimes of negative species [21,22] and charge exchange [23].

The resonator type of ion trap has several unique properties, such as the rapid slowdown of the stored ions near the turning points inside the electrostatic mirrors and the large focusing forces that are used to trap the ions. A particularity of the linear-trap resonator that arises from from these properties is the recently observed phenomenon of ion-motion synchronization [24], indicating that nontrivial dynamical effects can take place when a beam of charged particles is stored between two electrostatic mirrors.

In the original papers describing this type of trap [12,13], the stability criterion and the loss process were treated using a relatively simple model. In this paper we investigate the parameters that control the dynamical stability and trapping efficiency of these linear traps, and aim to provide a better understanding of the loss processes.

II. EXPERIMENTAL SETUP

In the present experiment, a beam of Ar^+ ions, with an initial kinetic energy of 4.2 keV, was produced by an electron-impact ion source. The ions were mass analyzed by a 20° magnet positioned adjacent to the ion source, and by an additional 45° magnet, located 5 m downstream. The ions were then injected into the ion trap, which was located 5 m away from the second magnet. The ion current was monitored with a Faraday cup located behind the trap and was of the order of 300 nA. Steering and focusing of the ions between the two magnets and between the last magnet and the ion trap was done with two electrostatic quadrupole triplet lenses. An electrostatic chopper located before the first magnet was used to create bunches of ions with a temporal extension of 1–100 μs.

A schematic drawing of the electrostatic ion trap is shown in Fig. 1. The mechanical design of the ion trap and its operation have been described previously [12,13]. Briefly, the ion trap consists of two coaxial electrostatic mirrors, each composed of a stack of eight cylindrical electrodes. The potentials of these electrodes are controlled independently, except for the innermost and outermost ones, which are always grounded. Thus, the central region between the two innermost electrodes with a length of 228 mm of the trap is essentially field-free. The diameter of the central hole is 16 mm in the outer six electrodes and 26 mm in the two innermost electrodes. The distance between the outermost electrodes is 407 mm. The trap is pumped by a cryopump, typically to a pressure of $\sim 5\times 10^{-10}$ Torr.

Injection of ions into the trap is realized by keeping the electrodes on one side of the trap at ground potential (left side in Fig. 1), while the electrode V_1 on the other side is kept at a potential that is high enough to reflect the ions. Before the ions return to the entrance side of the trap, the potentials of the electrodes on this side are rapidly (~ 100 ns) raised so that the ion bunch is confined between the two electrostatic mirrors. In the previous experiments performed with this setup [12,13,19–23], collimators of 1

*Author to whom correspondence should be addressed. FAX: +972-8-9344166. Email address: fndaniel@wicc.weizmann.ac.il

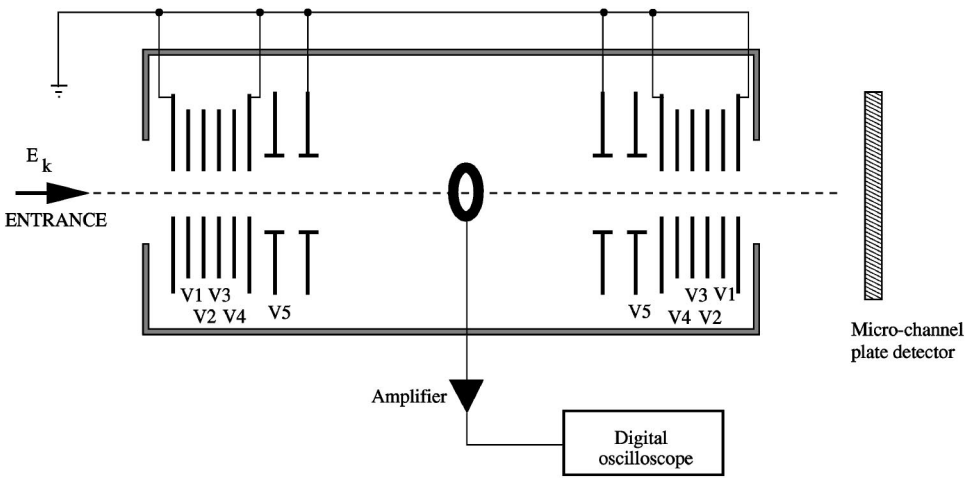

FIG. 1. Schematic view of the ion trap (not to scale). The bunch is injected through the left-hand side of the trap (entrance electrodes) and the neutralized Ar atoms are counted by the MCP detector located at the right side. The distance between the innermost electrode is 227 mm. The pickup electrode in the center is used to measure the intensity of the injected ion bunch.

and 2 mm diameter were located at the entrance and exit of the trap, respectively; while no collimators were used in the present setup.

In order for the ions to be trapped, the electrode electrical potentials have to satisfy certain conditions [12], which will be described in more detail in the following section. As various configurations of potentials are possible, we define a particular configuration by the vector $\{V_1,V_2,V_3,V_4,V_z\}$, which represents the potentials of the electrodes as shown in Fig. 1. The electrode connected to potential V_z in each mirror is called the Einzel electrode, as it plays a major role in defining the focusing properties of the ion trap [12,13]. In the present work, only symmetric configurations, where identical potentials are applied on each set of electrodes, are considered.

Once the bunch is stored, its evolution was monitored using a microchannel-plate (MCP) detector, located ~ 50 cm after the trap (see Fig. 1), which measures the number of neutral Ar^0 atoms emerging through the exit mirror. These atoms are produced in charge-exchange collisions with the residual gas inside the trap. A second detection device is a cylindrical pickup electrode of length $l_p=7$ mm with an inner diameter of 18 mm and a thickness of 1 mm, located at the center of the trap. The total capacitance of the pickup electrode, connectors, and vacuum feedthrough is $C_p \sim 10$ pF. When charged particles pass through the pickup, an image charge Q_p is induced on its surface. This charge is converted into a voltage V_A by a charge-sensitive amplifier. The amplifier was calibrated by injection of a known charge through a test capacitor using a voltage step with fast rise time ($\leqslant 20$ ns). The calibration showed a linear relation, $V_A=Q_p/C_f$, with $C_f=1.3$ pF. The output of the charge-sensitive amplifier is recorded on a digital oscilloscope, from which the number of injected ions can be evaluated. The pickup electrode was used to follow the time behavior of the injected bunch in the trap and a fast (~ 300 μs) debunching always occured with the present set of electrode potentials.

For stable trapping conditions, the rate of Ar^0 atoms exiting the trap and hitting the MCP detector is proportional to the number of ions trapped between the mirrors, so that the beam decay can be studied for different potential configurations of the electrodes. Many of these potential configurations lead to a stable condition for trapping; we have chosen a single set of voltages on the first four electrodes of each mirror, which create a nearly linear decrease of potential on the axis inside the mirror, namely, $V_1=6.5$ kV, $V_2=4.875$ kV, $V_3=3.25$ kV, and $V_4=1.625$ kV, while the voltage on the Einzel electrode was varied over a large range of values for which trapping could be achieved, i.e., $2.7<V_z<4.5$ kV.

III. RESULTS

Figure 2 shows an example for the measured number of Ar^0 atoms hitting the MCP for three different values of the Einzel electrode potential: $V_z=3.25$ kV (upper curve), $V_z=3.05$ kV (middle curve), and $V_z=4.15$ kV (lower curve). About 10^7 Ar^+ ions in a bunch of 5 μs were injected into the trap for each injection, and the data shown here are the sum over 100 injections. Similar decay curves were mea-

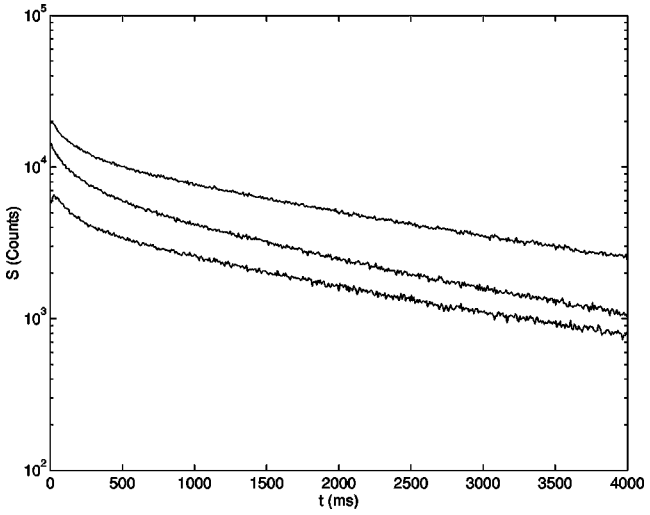

FIG. 2. Rate of neutral Ar atoms exiting the trap as measured by the MCP detector. The Einzel-electrode voltage was $V_z=3.25$ kV for the upper curve, $V_z=3.05$ kV for the middle curve, and $V_z=4.15$ kV for the lower curve. The data shown here are summed over 100 injections.

sured for other values of V_z. For all of these curves, an increase in the count rate was observed at short times ($t < 20$ ms). This is due to MCP saturation shortly after the injection flash. This region of the data was discarded in all further analysis. After the first 20 ms, the decay curves were characterized by a fast and a slow decaying part, as can be seen in Fig. 2, and in general, at least three different exponential decay times could be observed. It was also found that, although the major features of the decay curves were reproducible, the exact values of the decay times were injection dependent, i.e., a change in the focusing properties of the injection (quadrupole) optics influenced the slope of the decay curves.

The analysis of these curves is used to gain information on two important properties of the ion trap: The trapping efficiency ϵ_c and the loss processes. The former is defined as the ratio between the number of ions initially trapped N_T and the number of ions injected N_I. The number of injected ions can be estimated from the signal induced on the pickup electrode, but the number of stored ions is known only relatively through the number of neutral atoms hitting the MCP. As will be demonstrated later, not all ion-loss processes in the trap lead to neutralization (see Sec. V), so that not all the ions are counted by the MCP detector. However, a value proportional to the trapping efficiency can be obtained from the MCP signal: The number of ions measured by the MCP in a time interval Δt can be written as

$$S(t) = \alpha_c N(t) \Delta t, \tag{1}$$

where α_c is a constant of proportionality that accounts for the neutralization process, the MCP efficiency, and the geometrical acceptance of the detector, and $N(t)$ is the number of trapped ions at time t. Thus we can define a measured relative efficiency ϵ_m, proportional to ϵ_c, as

$$\epsilon_m = \alpha_c \epsilon_c = \alpha_c \frac{N(t=0)}{N_I} = \frac{S(t=0)}{\Delta t N_I}. \tag{2}$$

The measured signal at $t=0$ was found by extrapolation of the decay curve for $t<20$ ms. Figure 3(a) shows the value of ϵ_m as a function of the potential on the Einzel electrodes, V_z. There are clearly two regions of stability: $2.7 < V_z < 3.6$ kV and $4.0 < V_z < 4.3$ kV.

The loss processes that release the ions from the trap leave their mark in the details of the decay curves, shown in Fig. 2. However, because of the different number of decay constants needed to characterize these curves, we have chosen here to fit only the long-time behavior with a single exponent. A general fit to all the measured curves required a minimum of three decay constants, and would force us to adhere to a specific model describing the ion-loss processes. Figure 3(b) shows the results for the fitted decay constants of the slowly decaying part ($t>2$ s) as a function of V_z. It is important to point out that when a small collimator was placed at the entrance and exit sides of the ion trap, the decay curves were all well fitted by single exponents [13].

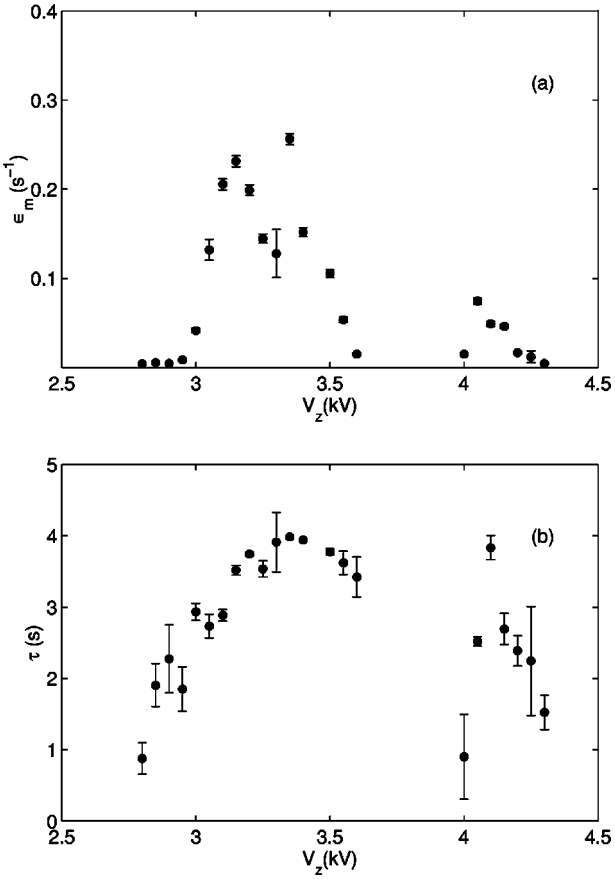

FIG. 3. (a) Measured relative efficiency ϵ_m as a function of the potential on the Einzel electrodes, V_z. (b) Fitted lifetime for the long-time behavior (for storage times >2 s) of the measured decay curves as a function of V_z.

IV. STABILITY AND TRAPPING-EFFICIENCY MODELS

In the following, we present two different models that are used to explain the basic factors affecting the stability and the trapping efficiency of the trap. It is the goal of this section to understand and reproduce the trapping efficiency shown in Fig. 3(a).

A. Trajectory calculations

One of the most straightforward ways to understand the trapping-efficiency behavior presented in Fig. 3(a) is to numerically perform classical trajectory calculations. For this purpose, we used the SIMION program [25], which can both solve the Laplace equation for a specific potential configuration in space and propagate ions on the computed potential grid. The program uses a fourth-order Runge-Kutta method to solve the Newtonian equation of motion. The density of ions is assumed to be low enough such that ion-ion interaction can be neglected, and the trajectories are calculated one ion at a time.

For each potential configuration of the electrodes there is an associated collection (E) of stable single-ion trajectories. The knowledge of this collection allows for a statistical analysis of the dynamical properties of the trap configuration. Considering that the trap is cylindrically symmetric and

that the total energy is conserved, all stable trajectories can be uniquely characterized by three phase-space coordinates $\{r,v_r,v_\theta\}$ on any plane ($z=$const) perpendicular to the axis of the trap, and their propagation for one reflection in the electrostatic mirror back to this plane. The cylindrical coordinates are the following: z is the distance from the center of the trap along the symmetry axis, r is the radial distance from this axis, and θ is the azimuthal angle, while v_z, v_r, and v_θ are the ion velocities in these directions. For convenience, we probe the phase space at the trap-center plane ($z=0$), where the ion kinetic energy equals the injection energy.

Using SIMION, the phase space was investigated for various values of the Einzel electrode potential V_z by propagating Ar^+ ions with an injection energy of 4.2 keV, while the initial coordinates $\{r,v_r,v_\theta\}$ were systematically varied.

A stable trajectory, defined as $S_i(r_i,v_{r_i},v_{\theta_i})$ was numerically identified by the requirement that a propagated ion was trapped for more than 500 μs ($\sim$200 oscillations), hence

$$E=\{S_i(r_i,v_{r_i},v_{\theta_i})|T_{f_i}>500\ \mu\text{s}\}, \tag{3}$$

where T_{f_i} is the duration of the trajectory i. The time limitation of 500 μs was found to be sufficient by making initial tests on a relatively large number of trajectories. It was found that for unstable trajectories, the ions were usually lost from the trap after a few oscillations ($\leqslant 20$ μs).

A first insight into the dynamics taking place in the trap can be gained by looking at selected trajectories inside the electrostatic mirrors for the two different regions of stability [see Fig. 3(a)]. Figures 4(a) and 4(b) show examples of such trajectories for $V_z=3.1$ kV and $V_z=4.1$ kV, respectively. The behaviors are clearly different. For $V_z=3.1$ kV, which exemplifies the lower region of stability, different trajectories with various distances y from the axis have turning points inside the mirror that are widely distributed radially, while in the higher region of stability, all trajectories focus close to the axis of the mirror.

To investigate the ion trajectories under realistic conditions of injection and electrode potentials, and to estimate the trapping efficiency, a Monte Carlo simulation type of calculation was performed. Briefly, for a given value of the Einzel-electrode potential, a sample N_S of ions was randomly chosen from an initial distribution of ions in phase space. These ions were then mapped onto the grid used to determine the phase space. The number of ions among the initial N_S mapped onto the phase-space element i is termed N_i, and the total number of trapped ions is $N_T=\Sigma_i N_i$, where the index i refers to the phase space of stable trajectories. Finally, we define a set of trajectory probabilities for the particular population of the phase space,

$$\varepsilon_i=\frac{N_i}{N_T}. \tag{4}$$

Note that $\Sigma\varepsilon_i=1$ always and for a homogenous filling of the trap $N_i=1$. All properties of the trajectories are then evaluated with these probabilities. Particularly, the trapping efficiency as defined in Sec. III is given by

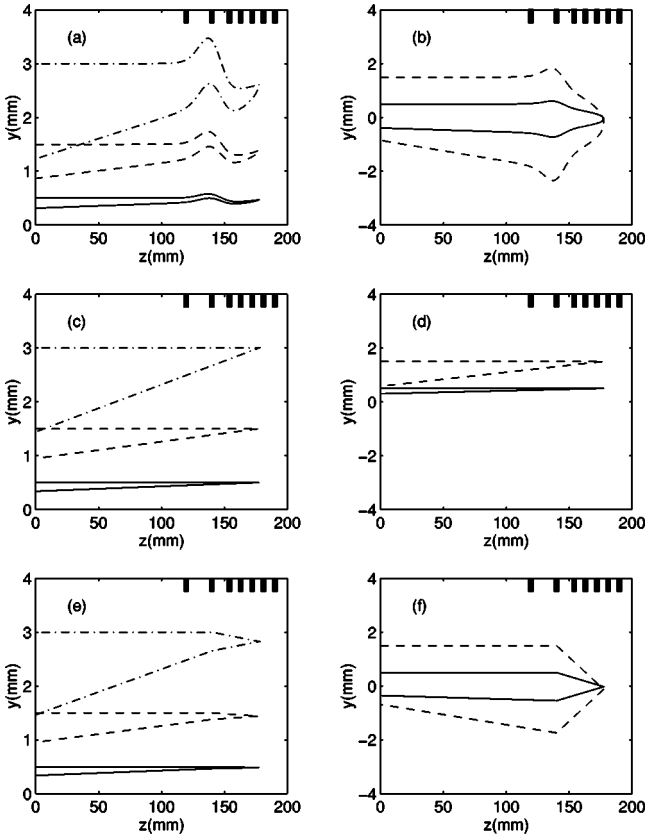

FIG. 4. Typical orbits of ions for various distances y from the axis. Upper panels: Trajectories as calculated using SIMION. (a) $V_z=3.1$ kV, (b) $V_z=4.1$ kV. Middle panels: Rays for the optical model 1. (c) $V_z=3.1$ kV, (d) $V_z=4.1$ kV. Lower panels: Rays for the optical model 2. (e) $V_z=3.1$ kV, (f) $V_z=4.1$ kV. The black rectangles at the top of each plot represent the positions of the electrodes.

$$\epsilon_c=\frac{N_T}{N_S}. \tag{5}$$

Results based on this procedure will be given in Sec. IV C.

B. The optical models

Although the stability and properties of the electrostatic trap can be evaluated directly by calculating the trajectories in the actual electrostatic potentials, useful insight can be gained by exploiting the analogy between light propagation in matter and propagation of charged particles in electric fields [12,13]. An optical model can provide a simple and intuitive understanding of the properties of the trap for a particular configuration. Also, the computational effort required with optical models is considerably less than with actual trajectory calculations, since ion propagation can be performed using the $ABCD$-matrix formalism developed in geometrical optics [26]. However, optical models cannot provide information about collision-induced properties (such as loss processes) and properties associated with nonplanar motion.

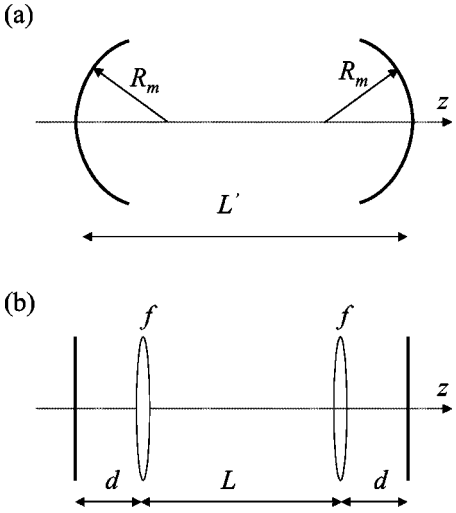

FIG. 5. Schematic drawing of the optical models: (a) model 1, (b) model 2.

1. Trap stability

The stability of the ion trap can be divided into two parts: axial and radial confinement. The first one is directly determined by the maximum potential on the trap axis U_{max},

$$\frac{E_k}{q} < U_{max}, \tag{6}$$

where E_k and q are the ion kinetic energy and electric charge, respectively.

It is possible to understand the radial stability of the trap when the analogy to an optical resonator is considered [12]. Previously, an optical model (model 1) of the present trap was presented where the entire electrostatic mirror was represented by a curved surface of reflection [12,13]. For a symmetrical optical resonator of this kind, and assuming that the mirrors are spherical with radius R_m, the radial-stability criterion is given by [12]

$$\frac{L'}{4} < f_m < \infty \quad \text{(model 1)}, \tag{7}$$

where L' is the effective length of the trap and $f_m = R_m/2$ is the focal length of the mirrors. Figure 5(a) shows a schematic drawing of such an optical resonator. In a later publication, Rockwood established the same criterion by simple physical arguments [27]. The qualitative validity of the stability conditions [Eqs. (6) and (7)] has been demonstrated experimentally [12,13]. However, the simplicity of the model is also its limitation when more precise and quantitative comparison is required. As will be shown later, some of the properties of the trapped beam, which can be observed in the trajectory calculations (see Sec. IV A), are not taken into account in this simple model.

A second model (model 2), which yields a better representation of the actual reflecting electrode assembly while remaining simple enough to be analyzed analytically, represents the reflecting electrostatic system as a lens of focal length f and a plane mirror located a distance d behind the lens. Figure 5(b) shows a schematic drawing of this model. In this model, it can be shown that there are two regions of stability for the focal length of the lens,

$$\frac{L}{2} \leqslant f \leqslant \infty, \tag{8}$$

$$\frac{dL}{2d+L} \leqslant f \leqslant d,$$

where L is the distance between the two lenses.

In order to use the optical models to deduce specific properties of the ion trap, the values of L' and f'_m for model 1 and L, d, and f for model 2 are needed for the different potential configurations of the trap electrodes. For this purpose, simple trajectory calculations, which required only one period of revolution were made. For model 1, the focal length f_m and the effective trap length L' are obtained by calculating the trajectories of ions initially moving parallel to the axis and observing both the position z_m, where the ions turn around (the mirror surface), and the position z_c, where they cross the optical axis after reflection. The difference between these two positions is defined as the focal length $f_m = z_m - z_c$ and $L' = 2z_m$.

For model 2, the parameters f, d, and L are determined similarly. The value of d is defined as the distance on the axis from the center of the Einzel electrode z_z to the position where the potential equals E_k/q of the ion. The focal length f can be obtained from the measurement of z_c and the position z_z of the Einzel electrode. With $\Delta z = z_z - z_c$, the focal length is

$$f = \Delta z + d \pm \sqrt{\Delta z^2 + d^2}, \tag{9}$$

where the minus sign before the square root applies if $f < d$.

At this point, it is instructive to compare the optical rays that can be traced for both optical models to the trajectories calculated with SIMION. The SIMION results are already shown in Figs. 4(a) and 4(b) for two typical values of the Einzel-electrode potential V_z ($V_z = 3.1$ kV and $V_z = 4.1$ kV), one for each region of stability shown in Fig. 3(a). For comparison, the optical-ray paths for the same Einzel-lens voltages are shown in Figs. 4(c) and 4(d) for model 1 and in Figs. 4(e) and 4(f) for model 2. There is a clear difference in the behavior of these rays and it is evident that model 2 gives a better representation of the trajectories than model 1. More specifically, and as pointed out in Sec. IV A, for the region of stability corresponding to large values of V_z, the focusing point in the mirror plane is independent of the radial distance, as calculated with SIMION. Thus, the direct benefit of model 2 as compared to model 1 is the prediction of very different dynamics in the two regions of stability. It is also important to point out that although model 1 does not predict two different regions of stability in terms of optical properties [see Eq. (7)], it does reproduce the two regions of stability in terms of the Einzel-electrode potential V_z: For model 1, a given focal length can be obtained for two different values of V_z, while this is not the case for model 2. It is obvious that the optical models can be ex-

tended even further, for instance, by allowing the mirror in model 2 to be curved, or by adding more optical elements.

When using optical models to calculate additional characteristics of the trap, such as trapping efficiency and ion density, spherical aberration needs to be taken into account. Since the stability criteria [Eqs. (7) and Eq. (8)] depend on the focal length, we consider the longitudinal spherical aberration, which is reflected in the dependency of the focal length (f_m or f) on the radial coordinate r. This dependency was investigated with SIMION by monitoring the change in the focal length for different trajectories, initially parallel to the axis, as a function of the radial distance r from this axis. For both models, it was found that the focal length can vary by a few orders of magnitude as a function of r, and that the focal length generally decreases for larger radial distances.

With the spherical aberration, the trap stability is evidently more complex and it is clear that the ion reflection at a large distance r from the axis is very different than close to the axis. The main difference between models 1 and 2 is that in the later, there is a well-defined region of stability for which the ions cross the optical axis ''inside'' the electrostatic mirror. This happens specifically for the Einzel-electrode voltage in the high region of stability in Fig. 3(a). In this region, the aberration is large, which hints to the fact that the stored beam will be more narrow than in the lower region of stability.

2. Simulations with the optical models

To evaluate explicitly the properties of the trap with the optical models, calculations in close analogy to these described for the SIMION simulation (see Sec. IV A) are performed using the $ABCD$-matrix formalism [26]. The $ABCD$ matrices including the aberrations calculated in Sec. IV B 1 are calculated from single trajectories when an ion is reflected only once in the electrostatic mirror. Thus, the propagation of the ion in the trap can be performed very rapidly, as once the $ABCD$ matrices are set for a specific configuration of the trap, only matrix multiplications are required. Another major difference from the SIMION simulation is that in both optical models, all orbits are planar, so that only two coordinates (r,v_r) are varied. The ion propagation is calculated for about 200 oscillations, starting with the same initial conditions as defined in Sec. IV A.

C. Results

The main function of the models described above is to provide an estimate of the trapping efficiency of the ion trap and to compare its dependence on V_z with the experimental data. The experimental data from Fig. 3(a), ϵ_m vs V_z, has been redrawn in Fig. 6(a) for better comparison with the calculations. Figures 6(b)–6(d) show the results (ϵ_c) of both the trajectory calculations [Fig. 6(b)] and the optical models [Fig. 6(c) for model 1 and Fig. 6(d) for model 2]. The efficiency has been calculated by representing the injected beam by a normal distribution for the coordinates x, y ($r=\sqrt{x^2+y^2}$), v_r, and v_θ for the trajectory calculation, and for the coordinates x, y, and v_r for the optical models. Three different distributions were chosen for the calculations: The

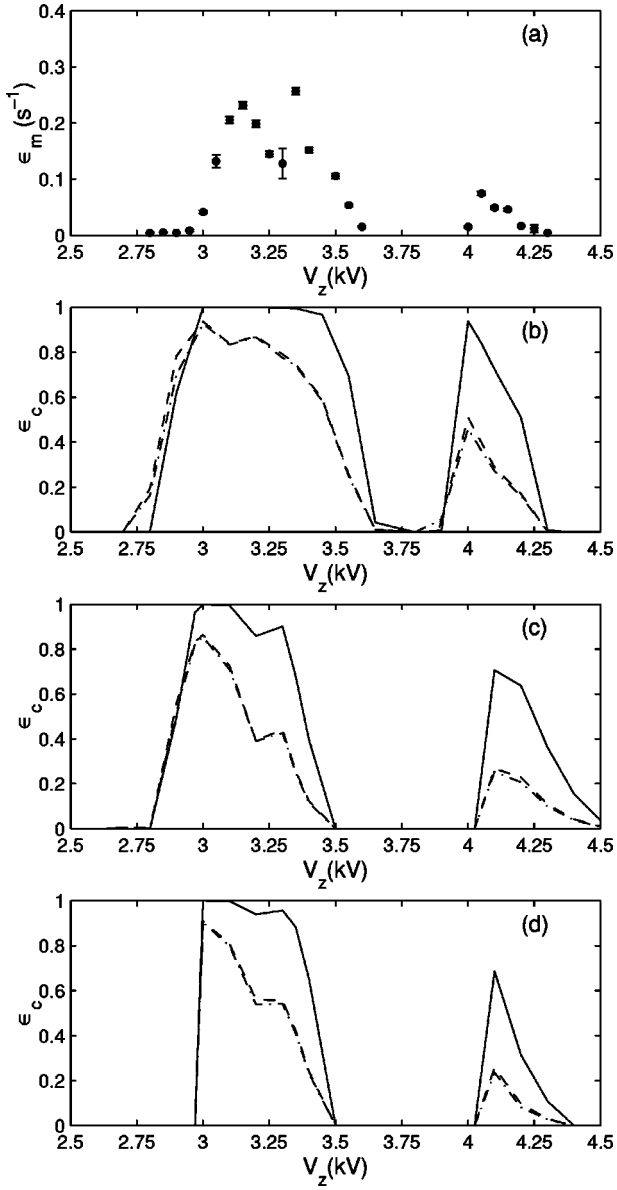

FIG. 6. Trapping efficiency versus V_z. (a) Measured relative trapping efficiency ϵ_m. (b) Calculated trapping efficiency ϵ_c using the trajectory calculation. (c) Calculated trapping efficiency ϵ_c using optical model 1. (d) Calculated trapping efficiency ϵ_c using optical model 2. For the calculated trapping efficiency the beam parameters were $\sigma(x)=\sigma(y)=1$ mm, $\sigma(v_r/v_t)=1$ mrad (continuous line); $\sigma(x)=\sigma(y)=2$ mm, $\sigma(v_r/v_t)=1$ mrad (dashed line); and $\sigma(x)=\sigma(y)=2$ mm, $\sigma(v_r/v_t)=2$ mrad (dot-dash line).

continuous line is for $\langle x\rangle=\langle y\rangle=\langle v_r\rangle=\langle v_\theta\rangle=0$ while the standard deviations were $\sigma(x)=\sigma(y)=1$ mm, $\sigma(v_r/v_t)=1$ mrad, and $\sigma(v_\theta/v_t)=0$, where v_t is the initial ion velocity. The dashed line is for a beam radius of $\sigma(x)=\sigma(y)=2$ mm and the rest of the parameters are unchanged. The dot-dash line is for a beam radius and an angular-velocity spread of $\sigma(x)=\sigma(y)=2$ mm and $\sigma(v_r/v_t)=2$ mrad, respectively, and the rest of the parameters are unchanged.

The two regions of stability $2.7<V_z<3.6$ kV and $4.0<V_z<4.3$ kV are well predicted by the trajectory calcula-

tions and by both optical models, and are in overall good agreement with the functional dependence of the experimental data over V_z. For a beam radius $\sigma(x)=\sigma(y)=1$ mm, the trapping efficiency reaches 100% in the lower region of stability ($3.0<V_z<3.5$ kV). For such a narrow beam, the efficiency in the higher region of stability reaches about 95% at 4.0 kV, but decreases rapidly for higher values of V_z. In general, the trajectory calculations [Fig. 6(b)] predict a larger region of stability than the optical models [Figs. 6(c) and 6(d)]. This is probably because the trajectories that are characterized by large angular momenta are not taken into account in the optical models. The region of low efficiency, below $V_z=3.0$ kV, which is predicted by the numerical calculations and by optical model 1, is not predicted by model 2. Also, in the higher region of stability, the optical models are slightly shifted toward higher values of V_z and they underestimate the trapping efficiency. It is expected that the real trapping efficiency is reduced by the fast transient voltages observed on the entrance mirror electrodes during several revolutions of the beam in the trap (tens of microseconds). In general, a larger beam is trapped with lower efficiency. On the other hand, an important point that can be learned from these results is that very high trapping efficiency can be obtained with such ion traps. An absolute comparison with the data is not possible at this point as the total number of ions stored in the trap is not known.

Additional insight can be gained by plotting the range of values of r at the center of the trap ($z=0$), for which trapping is possible, a value we define as the trapping radius. This is obtained by probing the whole phase space of the trap and recording the maximum and minimum radii for which stable trajectories exist. Figures 7(a)–7(c) show the trapping radius as a function of the Einzel-electrode potential V_z for the numerical simulation [Fig. 7(a)] and for optical model 1 [Fig. 7(b)] and model 2 [Fig. 7(c)]. The dependence of the trapping radius on V_z is mainly the result of the aberration, which is stronger for higher values of V_z. The trajectory simulation predicts that relatively large ion beams can be trapped, up to 5 mm radius at $V_z=3.1$ kV, with very good efficiency (see Fig. 6). For values smaller than $V_z=3.1$ kV, even larger beams can be trapped, but there is a minimum critical radius so that the trapped beam is hollow. However, with the present experimental system, the trapping efficiency for such beams is rather low (see Fig. 6). A hollow beam is also predicted at the lower edge of the higher region of stability. The comparison between the trajectory simulation and the optical models shows that these tend to underestimate the trapping radius. Model 1 predicts also the existence of hollow beams, in very good agreement with the trajectory simulation. The difference in trapping efficiency between the lower region of stability and the higher one (Fig. 6) can be understood in terms of the trapping radius. With the present configuration of electrodes and potentials, the maximum trapping radius in the region $4.0<V_z<4.4$ kV is smaller than for $3.0<V_z<3.6$ kV.

It is evident from Fig. 7 that neither of the optical models is completely consistent with the results of the trajectory calculations. As the angular momentum is not included in either of the optical models, the maximum trapping radius

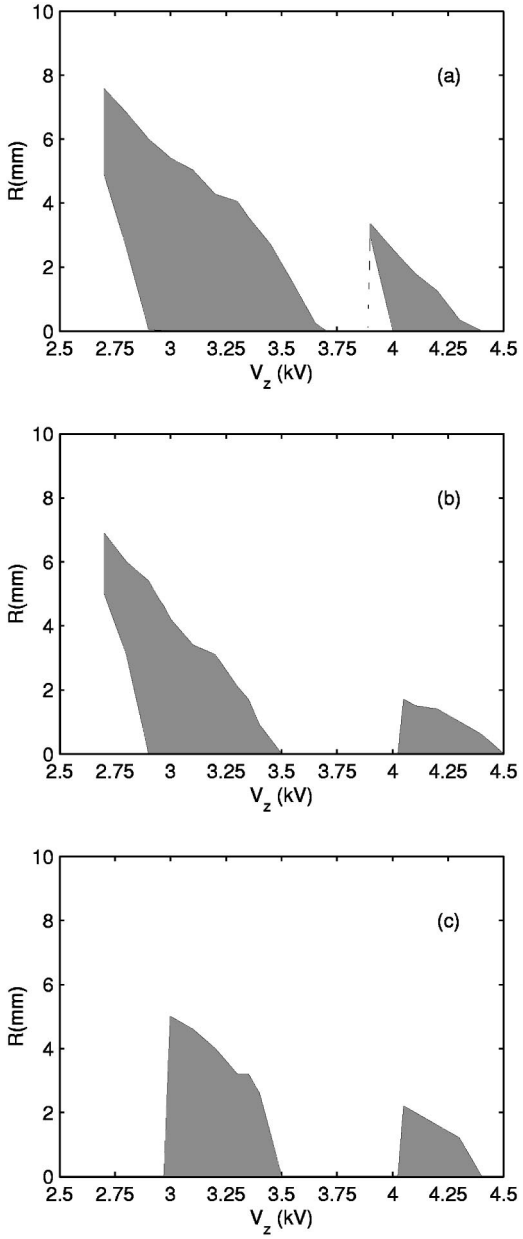

FIG. 7. Range of trapping radii as a function of the Einzel-electrode potential V_z for the numerical simulation (a), for optical model 1 (b) and for optical model 2 (c). The shaded areas represent the radius for which a stable beam can be stored.

predicted by these models will always be smaller. On the other hand, because of the simplicity of these models, and the small amount of computational effort required to obtain these results when compared to the long integration time needed to calculate the trajectories directly with SIMION (about 30 s for 500 μs of integration of a single trajectory on a Pentium III computer), these results serve as a useful first-order approximation for the trapping radius. Such calculations are important when experiments with merged beams (such as laser-ion-beam spectroscopy) are performed: It is then possible to adjust the trap configuration to optimize the overlap between the beams.

V. LOSS PROCESSES

In the preceding section we have addressed the question of the trapping efficiency as a function of the Einzel-electrode potential for one particular configuration of the other electrodes, while ignoring the details of the decay curves themselves (see Fig. 2). An ideal ion trap is a trap that can capture an ion beam with high efficiency and hold it for a long time. It is thus important to investigate also the details of the various ion-loss processes in the trap. In this section, we provide a detailed characterization of the various ion-loss mechanisms, which yield the multiexponential-decay curves seen in Fig. 2.

A. Ion-loss mechanisms

Trapped ions are lost due to collisions either with the residual gas or among the ions themselves. We consider two collision processes with a residual gas species R, namely, electron capture (I) (or electron loss for negative ions) and elastic or inelastic scattering (II), and we assume that further ionization of the trapped ions is negligible, a very good assumption for ions with energy of a few keV. For a beam of Ar^+ ions, processes (I) and (II) can be depicted as

$$\text{(I)} \quad Ar^+ + R^0 \rightarrow Ar^0 + R^+, \tag{10a}$$

$$\text{(II)} \quad Ar^+(\mathbf{p}_i) + R^0 \rightarrow Ar^+(\mathbf{p}_f) + R^0. \tag{10b}$$

In the first reaction, a trapped ion captures an electron from an atom or molecule R of the residual gas and exits the trap as a neutral atom. In the second reaction, the ion's initial momentum $\mathbf{p}_i$ is changed in the collision to $\mathbf{p}_f$, and the ion will be lost *if* scattered into an unstable orbit. Ion loss with this mechanism can occur both due to a single collision or as a result of multiple collisions.

A third ion-loss process (III) is the collisions among the stored particles, which can be depicted as

$$\text{(III)} \quad Ar^+(\mathbf{p}_1) + Ar^+(\mathbf{p}_2) \rightarrow Ar^+(\mathbf{p}_3) + Ar^+(\mathbf{p}_4), \tag{11}$$

and leads to ion loss upon scattering into unstable orbits. In Eq. (11), $\mathbf{p}_1$ and $\mathbf{p}_2$ are the initial momenta of two Ar^+ ions in the beam and $\mathbf{p}_3$ and $\mathbf{p}_4$ are their final momenta. We assume that charge exchange between two stored ions is a negligible process.

To quantify the description of collisions we define the probability P_i per revolution in the trap that an ion moving on trajectory i in phase space undergoes a collision of type X, where X describes one of the three ion-loss processes described above ($X = \text{I, II, III}$),

$$P_i = 1 - e^{-(\lambda_X)_i}, \tag{12}$$

where $(\lambda_X)_i$ is the average number of collisions in one revolution for the process X.

For reactions between ions and residual gas [processes I and II, Eq. (10)] the average number of collisions $(\lambda_{\text{I,II}})_i$ can generally be written as

$$(\lambda_{\text{I,II}})_i = n_G \int \sigma_{\text{I,II}}(v_i) v_i dt, \tag{13}$$

where n_G is the density of the residual gas, $\sigma_{\text{I,II}}(v_i)$ is either the capture (process I) or the scattering (process II) cross section as a function of the ion velocity v_i, and the integral is over one revolution of trajectory i. Similarly, for ion-ion scattering (process III) the average number of collisions in one revolution is

$$(\lambda_{\text{III}})_i = \int n_+ \sigma_{\text{III}}(\Delta v_i) \Delta v_i dt, \tag{14}$$

where n_+ is the density of ions and $\sigma_{\text{III}}(\Delta v_i)$ is the cross section for scattering of ions with relative velocities Δv_i. Each of the three ion-loss processes will now be treated separately.

1. Electron capture

The cross section for electron capture, σ_{I} has only a weak dependence on energy up to keV energies [28] and we assume it to be constant for the energy range present in the trap. Under this assumption, the average number of electron-capture events during one revolution of ion i in the trap can be written explicitly,

$$(\lambda_{\text{I}})_i = k \frac{\sigma_I P}{T} \int v_i dt, \tag{15}$$

where k is a constant [$k = 9.656 \times 10^{18}$ K/(cm^3 Torr)], P is the residual gas pressure (in Torr), and T is the temperature (in kelvin). Using SIMION, it was found that the integral in Eq. (15) was constant for different values of the Einzel-electrode potential, with a very weak dependence on the initial values used in the trajectory calculations, as defined in Sec. IV A. This can easily be understood as this integral represents the length of the trajectory, which is not strongly influenced by the value of V_z nor by the initial values.

With realistic numbers for the present experimental system, $P \sim 5 \times 10^{-10}$ Torr, $T \sim 300$ K, $\sigma_{\text{I}} \sim 10^{-15}$ cm^2 [28], and an effective trajectory length of 35.5 cm, a value of $\lambda_{\text{I}} \sim 6 \times 10^{-7}$ is obtained. For a 4.2-keV Ar^+ beam, a revolution in the trap is ~ 3 μs, yielding a decay rate of $k_{\text{I}} \sim 0.2$ s^{-1}, or a corresponding lifetime of $\tau_{\text{I}} = 5$ s.

2. Ion-neutral scattering

A quantitative estimate of the influence of ion-neutral scattering on the loss of trapped ions requires the evaluation of both the scattering cross section and the maximum angle of scattering for which the beam is still trapped, a value we define as the angular acceptance. The angular acceptance will be considered in more detail in Sec. V A 4 based on trajectory calculations. Here we note that the acceptance angle in the center of the trap is of the order of 1 mrad.

Absolute differential cross sections for scattering at keV energies have been measured for several systems, in particular, for H [29] and O [30] atoms scattered on rare gases. Such data are relevant (taking into account that in the center-of-mass frame of reference, the target and projectile are

''equivalent'') to the present situation, where it is a rare-gas atom (Ar) that is scattered on the residual gas, which is mainly made of H_2 and H_2O molecules. For instance, when 1.5-keV O atoms (i.e., with a relative velocity of 134.1 mm/μs) were scattered on a stationary target of Ar, the integral cross section for scattering into laboratory angles of 3.49 mrad$\leqslant\theta_L\leqslant$107.5 mrad was measured to be 1.08×10^{-15} cm^2. The corresponding angular range when Ar acts as the projectile would be 1.4 mrad$\leqslant\theta_L\leqslant$43.0 mrad, i.e., well above the typical acceptance angle of the ion trap. The fact that the measurements made in Refs. [29,30] were performed for both neutral projectiles and targets is in fact yielding a lower limit for the ion-neutral-scattering cross section, as charged particles would increase the scattering angles. Thus, the loss of ions by ion-neutral scattering is an important process in this trap and is equivalent in its strength to the electron-capture cross section.

To obtain a general estimate, the interaction between the two colliding atoms can be represented by a Fermi-Thomas potential [31], and becomes explicitly

$$\frac{d\sigma}{d\Omega}=\frac{\sigma}{\pi}\frac{\theta_{min}^2}{(\theta_{min}^2+\theta^2)^2}, \tag{16}$$

where σ is the total scattering cross section and $\theta_{min}=\hbar/(\mu v a)$ is the minimum angular deflection for a system with reduced mass μ, relative velocity v, and atomic radius a. Within this model the total scattering cross section is known to be proportional to $1/v^2$ [31].

Thus, for ion scattering on the residual gas, the average number of collisions in one revolution can be estimated as [see Eq. (13)]

$$(\lambda_{\mathrm{II}})_i=k\frac{\sigma_{\mathrm{II}}(v_0)v_0^2P}{T}\int\frac{dt}{v_i}, \tag{17}$$

where $\sigma_{\mathrm{II}}(v_0)$ is the scattering cross section at a known velocity v_0 that leads to scattering into angles larger than the acceptance angle.

The effect of the electrode electrical configuration of the trap and the population of the phase space on λ_{II} is represented by the integral of the inverse ion velocity. For each of the studied electrical configurations, this integral was calculated with SIMION for each trajectory in the phase space. The average value of the integral was typically 0.05 μs^2/mm but clearly depended on the potential of the Einzel electrode. Moreover, the widths of the distributions of this integral varied between 0.01–0.02 μs^2/mm while varying V_z.

The average time between ion-neutral collisions that leads to loss can be estimated from Eq. (17): for a cross section $\sigma_{\mathrm{II}}(v_0)=10^{-15}$ cm^2, $v_0=1.4\times10^7$ cm/s, $P=5\times10^{-10}$ Torr, $T=300$ K, and taking the value of the integral as 0.5×10^{-12} s^2/cm, a value of $\lambda_{\mathrm{II}}=1.6\times10^{-6}$ is obtained, which corresponds to an average time between such collisions of $\tau_{\mathrm{II}}=1.8$ s. Such a time is of the same order of magnitude as the lifetime observed in the trap.

A direct implication of the importance of the ion-neutral scattering is that since the average number of collisions λ_{II} is described by a distribution that is both dependent on V_z and the trajectory, the ion loss due to the ion–residual gas scattering will be manifested in the measured decay curve with multiple slopes, or, in general, with nonexponential behavior, which will be sensitive to the exact values of the electrode potential and injection conditions. However, for long storage times, a steady-state distribution is reached and the decay is exponential.

3. Ion-ion scattering

The ion-ion scattering in the trap is an important process only in regions where the ion density n_+ is large [see Eq. (14)], which happens in the regions where the ion velocity is small, i.e., near the turning points. Thus, to a first approximation $(\lambda_{\mathrm{III}})_i$ will be approximated by its incremental value at these points. Consider a small temporal segment δt of the trapped ion beam. In the center of the trap this segment is characterized by a longitudinal size $\Delta z_0=v_0\delta t$ and a radial extension R_0. Between electrodes V_1 and V_2 (Fig. 1), where the ions turn around, the segment is longitudinally contracted due to the deceleration to a size Δz_t, while the radial size is changed to R_t, according to the focusing properties of the trap. In general, the ion density at the turning points, $(n_+)_t$, can be written as

$$(n_+)_t=(n_+)_0\left(\frac{R_0}{R_t}\right)^2\left(\frac{\Delta z_0}{\Delta z_t}\right), \tag{18}$$

where $(n_+)_0$ is the ion density on the center of the trap. The beam radii R_0 and R_t can be evaluated directly from the phase-space calculation (see Sec. IV A), while Δz_t can be estimated by a second-order expansion of the position of the segment around the turning point,

$$\Delta z_t=\frac{1}{3}\left(\frac{\delta t}{2}\right)^2\left(\frac{q}{M}\right)\left(\frac{dU}{dz}\right)_t, \tag{19}$$

where q and M are the ionic charge and mass, respectively, and $(dU/dz)_t$ is the axial gradient of the electrostatic potential at the turning point.

Assuming that the ion-ion-scattering cross section behaves as $1/\Delta v^2$ [31], where Δv is the relative velocity between two ions, the average number of ion-ion collisions during one revolution can be written as [see Eq. (14)]

$$(\lambda_{\mathrm{III}})_i=k'(n_+)_0\sqrt{\frac{MU_0}{q}}\sigma_{\mathrm{III}}(\Delta v_0)\Delta v_0^2\left(\frac{dU}{dz}\right)_t^{-1}\left(\frac{R_0}{R_t}\right)^2\left\langle\frac{1}{\Delta v_i}\right\rangle, \tag{20}$$

where U_0 is the acceleration voltage, $\sigma_{\mathrm{III}}(\Delta v_0)$ is the ion-ion-scattering cross section at a known relative velocity Δv_0, and $\langle 1/\Delta v_i\rangle$ is averaged over the phase space at the turning points. Equation (20) demonstrates that the average number of ion-ion collisions per revolution in the trap is a function of both the electrical configuration of the electrodes, through the value of $(dU/dz)_t$, and the specific population of phase

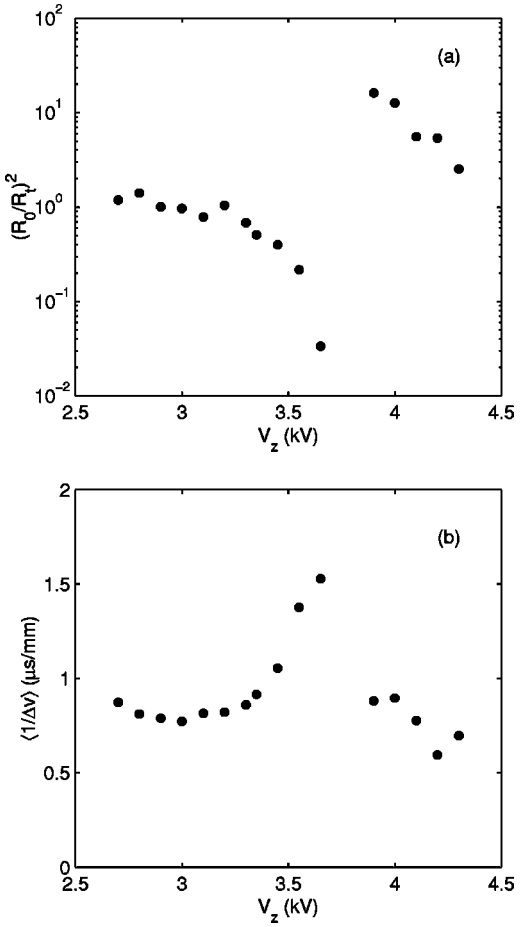

FIG. 8. (a) Square of the radial compression at the turning point of the ion trap as a function of V_z. (b) Value of $\langle 1/\Delta v \rangle$ at the turning points as a function of V_z.

space, through the (R_0/R_t) and $\langle 1/\Delta v_i \rangle$ factors, which are also functions of the electrode potentials.

The significance of each of these factors was investigated through calculations with SIMION. Since only the potential of the Einzel electrode was varied, the value of $(dU/dz)_t \sim 165$ V/mm can be considered constant in the present study. Figure 8(a) shows the square of the ratio between the beam radius at the center of the trap, R_0, and the beam radius at the turning point, R_t, as a function of the Einzel-electrode potential as calculated for the homogeneous beam. It can be seen that this ratio is strongly dependent on V_z, and that around 3.75 kV, a radial compression factor of about three orders of magnitude is obtained. At the same time, the average value of $1/\Delta v$, shown in Fig. 8(b), is increasing up to $V_z = 3.6$ kV. Since the average number of ion-ion collisions λ_{III} is a strong function of V_z and is trajectory dependent, nonexponential behavior in its contribution to the measured decay curves can be expected. The widths of the distributions of $1/\Delta v_i$ were found to be as large as 0.25–0.5μs/mm for the various electrical configurations, and with such widths a strong influence of the initial beam shape on the decay curves can be expected.

An estimate of the average time between ion-ion collisions, for a beam density of 10^6 cm^{-3}, using Eq. (20) and typical parameters of our system, yields a value of $\tau_{\mathrm{III}} = 350$ ms. However, not all ion-ion collisions lead to the loss of ions from the trap, and here also, as for the ion-neutral scattering, a better estimation of the influence of λ_{III} on the lifetime of the trapped beam requires the evaluation of the angular acceptance. Nevertheless, it is interesting to point out that this value is of the same order of magnitude as the time scale in the decay curves for which nonexponential behavior is observed (see Fig. 2).

4. Acceptance angle

When considering the significance of the scattering processes [processes II and III, Eqs. (10b) and (14)] for ion loss in the electrostatic trap, the stability of each trajectory towards angular deflection must also be evaluated.

At a particular segment $[S_i; S_i + dS_i]$ of trajectory i the distribution of angles relative to neighboring stable trajectories is given by the available phase space

$$(\theta_r)_i = \arccos\left(\frac{\mathbf{v}_i \cdot \mathbf{v}_j}{v_i v_j}\right), \tag{21}$$

where j runs over the neighboring orbits. This equation is valid for both ion–residual gas scattering and ion-ion scattering.

A measure of the angular acceptance can be calculated by estimating the width of the distribution of θ_r as obtained from Eq. (21) for a large number of trajectories. It was found that such a distribution is sensitive to both the radial distance from the axis of the trap and to the distance z from its center.

Figure 9(a) shows the values of the average acceptance angles $\langle \theta_c \rangle$ as obtained from the standard deviation of the distribution of θ_r at the center of the trap ($z = 0$). Figure 9(b) shows the same at the turning point $\langle \theta_t \rangle$, where the ion-ion scattering is dominant, as a function of the Einzel-electrode potential. As can be seen there is a huge difference in the value of the acceptance angles: while it is in the milliradian range at the center of the trap, it is almost three orders of magnitude larger at the turning point. This does not mean that the ion-loss process due to scattering from the residual gas near the turning point is unimportant; the kinetic energy of the ions in that region is very low and large angles of scattering are possible. In any case, the dependence of $\langle \theta_c \rangle$ and $\langle \theta_t \rangle$ on V_z at both the center and at the edges of the trap is quite strong, and it is expected that the beam lifetime is directly affected by these changes.

The widths of the distibutions of acceptance angles were seen to be of the order of 1–2 mrad for θ_c and 0.2–0.4 rad for θ_t depending on the different electrical configurations. For trajectories close to the edges of stabillity in phase space, the acceptance angles approach zero.

The acceptance angles as plotted in Figs. 9(a) and 9(b) are evaluated in the laboratory frame of reference. If the projectile mass M_i (ion mass) is larger than the target mass M_R (mass of the neutral gas atoms or molecules), there is a maximum angle of scattering given by

$$\theta_{max} = \arcsin(M_R/M_i), \tag{22}$$

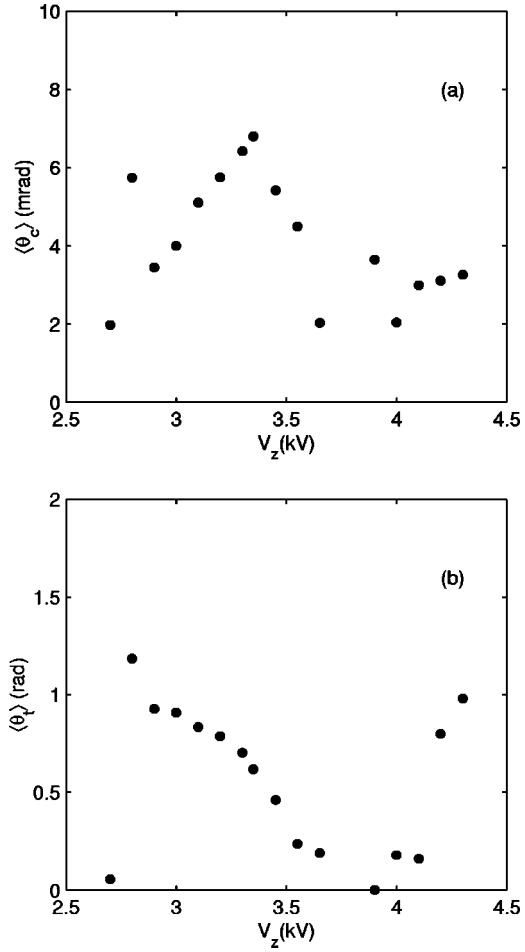

FIG. 9. Average acceptance angles as a function of V_z: (a) at the center of the trap; (b) at the turning point. Note the difference in units.

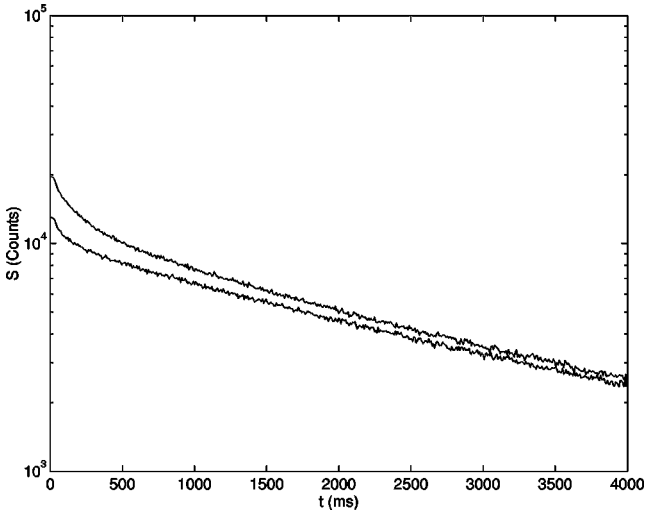

FIG. 10. Rate of neutral Ar atoms exiting the trap as measured by the MCP detector for a high-intensity beam (upper curve) and a low-intensity beam (lower curve). The Einzel-electrode voltage was $V_z = 3.25$ kV. The data shown here are summed over 100 injections.

which might be always smaller than the acceptance angle. In such a case, a single scattering event cannot lead to the loss of an ion. In the case of Ar^+ impinging on H_2, which is the dominant residual gas in the trap, $\theta_{max} = 50$ mrad, well below the value of $\langle \theta_t \rangle$ at the turning point of the trap [see Fig. 9(b)]. If only one type of ion is stored in the trap (as in the present case), this kinematical effect has no influence on the ion-ion scattering. However, in the case where two different masses are stored together [32], subtle effects due to collisions between the lighter and heavier mass can appear in the decay curves.

In general, we find that the ion-loss rate due to scattering (processes II and III) is a complicated function of the exact trajectory of the stored ion inside the trap, and that a full understanding requires extensive calculations.

B. Ion-loss processes: Comparison to experimental data

Among the three loss processes described above, the ion-ion scattering is the only one that depends directly on the ion density. One can thus expect that its influence on the decay curve is limited to short times, though this does not mean that the other ion-loss processes do not influence the short-time-decay rates. It is difficult to give a quantitative time scale, since the dependence of this process on the trap configuration is very strong, as can be seen through the radial compression ratio [Fig. 8(a)], the change in the average of the inverse relative ion velocity [Fig. 8(b)], and the acceptance angles (Fig. 9). A complete Monte Carlo simulation is needed to understand the intricate contribution of each of these factors. However, because of the dependence of the ion-loss process due to ion-ion collisions on the ion density, a lessening of its influence should be observable when injecting weaker beams into the trap. For this purpose, we have measured decay curves under the same experimental conditions (i.e., residual pressure and all electrode potentials) but with different beam intensity. The intensity reduction was performed by closing a set of slits located between the two magnets, about 7 m upstream from the ion trap. The result is shown in Fig. 10, where the upper curve is for 100 injections of 10^7 ions each and the lower curve is for 100 injections of 5×10^6 ions at $V_z = 3.25$ kV. The short-time behavior is different: the fast decay present in the higher-intensity beam is much weaker in the lower-intensity injections. In a recent work [24], we showed that by selecting a special set of electrode potentials the ion-ion scattering contribution can be increased to the point where collective effects such as synchronization of the ion motion can be observed.

The long-time behavior of the decay curves, which is shown in Fig. 3(b), also shows a dependence on the Einzel-electrode potential. Two factors influence this part of the decay curve. The first one is the electron-capture process, which is independent of the electrode-potential configuration. The second one is the ion–residual gas scattering, which shows strong dependence on V_z. We still cannot reproduce the experimental data shown in Fig. 2, but it seems that the dominant factor is the dependence of the acceptance angle upon the Einzel-electrode potential (see Fig. 9). The acceptance angle at the center of the trap is maximum for $V_z = 3.4$ kV, and the lifetime (see Fig. 2) is also the longest

for the same voltage, leading to the conclusion that ion-neutral scattering is a significant loss process for long-time storage. However, a complete understanding of the lifetime behavior will require a detailed knowledge of the competition between the different factors affecting the scattering probability and the acceptance angle along the axis of the trap.

An interesting point is a comparison with previous measurements [13] done with the same trap, where the beam was injected through a 1-mm-diameter collimator and the exit side of the trap was also restricted by a 2-mm collimator located on the last electrode. With this setup, single exponential decay was observed, with very weak dependence on the Einzel-electrode potential. Also, much shorter lifetimes, at comparable residual-gas pressure, were observed. This result can be explained by the fact that (1) the initial collimation reduced the total number of ions injected into the trap to much lower values, hence reducing the effect of ion-ion scattering and (2) the exit collimator only permitted observation of the trapped beam close to the axis. Since ion–residual gas scattering always tends to increase the radius of the beam, the measured decay constant (observed through the electron-capture process) was geometrically correlated to the central part of the beam. The lifetimes measured were shorter because the ion–residual gas scattering moved the ions out of the line of sight of the MCP detector. In fact, these ions were not lost from the trap and the real lifetime is about an order of magnitude longer than that measured in Ref. [13].

VI. CONCLUSIONS

In this work we have measured the relative trapping efficiency as well as the lifetime of an Ar^+-ion beam at an energy of 4.2 keV in a linear electrostatic ion trap as a function of the electrical configuration of the trap. We have presented trajectory calculations as well as optical models, which reproduce the functional dependence of the trapping efficiency and explain the complexity of the ion-loss processes. We found that three mechanisms contribute to the loss of ions: charge-exchange, ion-ion, and ion–residual gas scattering. We have tried to parametrize the most important factors affecting the trapping efficiency and beam lifetime of such a trap. From our results, it is clear that different trap geometries and potential configurations on the electrodes will change the exact values, and that optimization of all these parameters can yield ion traps with even longer lifetimes.

Linear ion traps of the type described here are capable of very high trapping efficiencies, which can theoretically reach 100%. It is still left to perform a quantitative measurement that shows such efficiency, but from the data presented and from other experiments where beam extraction from the trap was performed [13], it is clear that the trapping efficiency is of the order of many tens of percent. Such an order of magnitude has also recently been obtained with the CONETRAP [15], in which an estimated 30% of the beam was trapped. Good collimation of the beam prior to injection is essential to achieve high trapping efficiency; this can be obtained using standard ion optics upstream of the trap.

The optical models developed here have been demonstrated to characterize well the ion trap and can be used to explain the trapped-beam behavior, such as trapping radius as well as trapping efficiency. The main difference between model 1 and model 2 is the trajectory representation inside the mirror electrodes, where clearly model 2 is superior. These tools can now be used to perform preliminary optimization before the exact design of such a trap is undertaken. These models are also useful for optimizing the potential configuration of the electrodes to obtain a specific beam size inside the trap.

In Sec. V we showed that the determination of the beam lifetime in such a trap is a complex issue related to the electrical configuration of the trap. Although we studied the dependence of the decay rates on V_z only, it is clear that different potentials on the other electrodes will also lead to a change in the beam lifetime. A complete Monte Carlo simulation is needed to reproduce the decay curves. An additional conclusion is that when this type of ion trap is used to measure lifetimes of atomic metastable states, care should be taken to either correct for the nonexponential behavior of the number of stored ions with time, or use a specific setup (geometrical and electrical) that will produce a single exponential decay. In general, we conclude that the scattering process of the ions on the residual-gas atoms or molecules is the dominant ion-loss process at long times.

An important effect that is taking place when special electrical configurations are used is ion-motion synchronization, which allows a packet of ions to be stored with a constant length for a time that is much longer than the standard diffusion time [24].

ACKNOWLEDGMENTS

This work was supported by the German Ministry of Education, Science, Research and Technology (BMBF) within the framework of the German-Israeli Project Cooperation in Future-Oriented Topics (DIP), by the Alhadeff Foundation, by the Minerva Foundation, by a special grant from Yeda, and by the European Union under the Fifth Framework program, Contract No. HPRN-CT-2000-00142.

[1] For a review of ion traps, see, e.g., Proceedings of Nobel Symposium 91, edited by I. Bergström, C. Carlberg, and R. Schuch [Phys. Scr. T **T59** (1995)].
[2] W. Paul, W. Oberghaus, and E. Fischer, Forschungsber. Wirtsch.-Verkehrminist. Nordrhein-Westfalen **415**, 1 (1958).
[3] W. Paul, Rev. Mod. Phys. **62**, 531 (1990).
[4] F.M. Penning, Physica (Amsterdam) **3**, 873 (1936).
[5] H. Dehmelt, Rev. Mod. Phys. **62**, 525 (1990).
[6] N. Yu, W. Nagourney, and H. Dehmelt, J. Appl. Phys. **69**, 3779 (1991).
[7] C.A. Schrama, E. Peik, W.W. Smity, and H. Walter, Opt. Commun. **101**, 32 (1993).

[8] K.H. Kingdon, Phys. Rev. **21**, 408 (1923).
[9] D.A. Church, Phys. Scr., T **T59**, 216 (1995).
[10] R. Blümel, Phys. Rev. A **51**, R30 (1995).
[11] R. Blümel, E. Bonneville, and A. Carmichael, Phys. Rev. E **57**, 1511 (1998).
[12] D. Zajfman, O. Heber, L. Vejby-Christensen, I. Ben-Itzhak, M. Rappaport, R. Fishman, and M. Dahan, Phys. Rev. A **55**, R1577 (1997).
[13] M. Dahan, R. Fishman, O. Heber, M. Rappaport, N. Altstein, W.J. van der Zande, and D. Zajfman, Rev. Sci. Instrum. **69**, 76 (1998).
[14] W.H. Brenner, Anal. Chem. **69**, 4162 (1997).
[15] H.T. Schmidt, H. Cederquist, J. Jensen, and A. Fardi, Nucl. Instrum. Methods Phys. Res. B **173**, 523 (2001).
[16] S. Datz (private communication).
[17] X. Urbain (private communication).
[18] S.P. Møller, Nucl. Instrum. Methods Phys. Res. A **394**, 281 (1997).
[19] R. Wester, K.G. Bhushan, N. Altstein, D. Zajfman, O. Heber, and M.L. Rappaport, J. Chem. Phys. **110**, 11 830 (1999).
[20] K.G. Bhushan, H.B. Pedersen, N. Altstein, O. Heber, M.L. Rappaport, and D. Zajfman, Phys. Rev. A **62**, 012504 (2000).
[21] A. Wolf, K.G. Bhushan, I. Ben-Itzhak, N. Altstein, D. Zajfman, O. Heber, and M.L. Rappaport, Phys. Rev. A **59**, 267 (1999).
[22] L. Knoll, K.G. Bhushan, N. Altstein, D. Zajfman, O. Heber, and M.L. Rappaport Phys. Rev. A **60**, 1710 (1999).
[23] D. Strasser, K.G. Bhushan, H.B. Pedersen, R. Wester, O. Heber, A. Lafosse, M.L. Rappaport, N. Altstein, and D. Zajfman, Phys. Rev. A **61**, 060705 (2000).
[24] H. B. Pedersen, D. Strasser, S. Ring, O. Heber, M. L. Rappaport, Y. Rudich, I. Sagi, and D. Zajfman, Phys. Rev. Lett. **87**, 055001 (2001).
[25] SIMION, Version 6.0, Ion Source Software.
[26] See, e.g., R. Guenther, *Modern Optics* (Wiley, New York, 1990).
[27] A.L. Rockwood, J. Am. Soc. Mass Spectrom. **10**, 241 (1999).
[28] G.J. Lockwood, Phys. Rev. A **2**, 1406 (1970).
[29] R.S. Gao, L.K. Johnson, K.A. Smith, and R.F. Stebbings, Phys. Rev. A **40**, 4914 (1989)
[30] G.J. Smith, R.S. Gao, B.G. Lindsay, K.A. Smith, and R.F. Stebbings, Phys. Rev. A **53**, 1581 (1996).
[31] J. D. Jackson, *Classical Electrodynamics*, 2nd ed. (Wiley, New York, 1975).
[32] S. Ring, H.B. Pedersen, O. Heber, M.L. Rappaport, P.D. Witte, K.G. Bhushan, N. Altstein, Y. Rudich, I. Sagi, and D. Zajfman, Anal. Chem. **72**, 72 (2000).